

## Molecular Interaction Fields and 3D-QSAR Studies of p53–MDM2 Inhibitors Suggest Additional Features of Ligand–Target Interaction

Cristina Dezi,<sup>†</sup> Andrea Carotti,<sup>†</sup> Matteo Magnani,<sup>‡</sup> Massimo Baroni,<sup>§</sup> Alessandro Padova,<sup>‡</sup> Gabriele Cruciani,<sup>§,||</sup> Antonio Macchiarulo,<sup>\*,†</sup> and Roberto Pellicciari<sup>†</sup>

Dipartimento di Chimica e Tecnologia del Farmaco, Università di Perugia, via del Liceo 1, 06123 Perugia, Italy, Siena Biotech S.p.A., Strada del Petriccio e Belriguardo, 35, 53100, Siena, Italy, Molecular Discovery Ltd, 215 Marsh Road, Pinner, Middlesex HA55NE, England, and Laboratory for Chemometrics and Cheminformatics, Department of Chemistry, Università di Perugia, via Elce di Sotto 10, 06123 Perugia, Italy

Received March 24, 2010

The design and optimization of small molecule inhibitors of the murine double minute clone 2–p53 (p53–MDM2) interaction has attracted a great deal of interest as a way to novel anticancer therapies. Herein we report 3D-QSAR studies of 41 small molecule inhibitors based on the use of molecular interaction fields and docking experiments as part of an approach to generating predictive models of MDM2 affinity and shedding further light on the structural elements of the ligand–target interaction. These studies have yielded predictive models explaining much of the variance of the 41 compound training set and satisfactorily predicting with 75% success an external test set of 36 compounds. Not surprisingly, and in full agreement with previous data, inspection of the 3D-QSAR coefficients reveals that the major driving force for potent inhibition is given by the hydrophobic interaction between the inhibitors and the p53 binding cleft of MDM2. More surprisingly, and challenging previous suggestions, the projection of the 3D-QSAR coefficients back onto the experimental structures of MDM2 provides an intriguing hypothesis concerning an active role played by the N-terminal region of MDM2 in ligand binding.

### INTRODUCTION

The oncogenic protein murine double minute clone 2 (MDM2) is an E3 ubiquitin ligase enzyme that plays a pivotal role in regulating the transcriptional activity of the tumor suppressor factor p53.<sup>1</sup> This is operated by the binding of MDM2 to the transactivation domain of p53 promoting an inhibition of the transcriptional activity of p53 and targeting p53 to proteosomal degradation.<sup>2</sup> More than 800 human cancers with wild-type p53 have been reported, as characterized by altered expression of MDM2 and/or MDMX,<sup>3–12</sup> its homologue oncogenic protein.

In view of these data and given the inhibitory role fulfilled by MDM2 in the p53 pathway, the development of inhibitors of the p53–MDM2 interaction with drug-like properties has become a major topic in drug discovery programs aimed at disclosing novel anticancer therapies.<sup>13,14</sup>

As a consequence, considerable efforts have been devoted over the past decade to the structural and computational characterization of the interaction between MDM2 and p53 in order to provide clues for the design of peptides and/or small molecules able to block the formation of the p53–MDM2 complex. Structural studies, in particular, have provided a number of crystal and NMR structures of apo-, p53-, peptide-, and small molecule-bound MDM2 complexes.<sup>15–26</sup>

Starting from these experimental observations, computational studies have then investigated the conformational space of the p53 binding cleft<sup>27–33</sup> and the stability of wild-type p53 and mutants<sup>34,35</sup> as well as the binding affinity of short peptides to MDM2.<sup>36–38</sup> Overall, these studies pinpoint the presence of three flexible hydrophobic pockets in the MDM2 structure constituting a transient hollow binding site that is amenable to structure-based drug design (SBDD) strategies.<sup>39</sup>

On this basis, a great deal of research has been devoted to the identification of p53–MDM2 inhibitors through the screening of chemical libraries and design of peptidomimetics.<sup>40–45</sup> This has provided distinct classes of active compounds (**1–6**, Figure 1) that feature common pharmacophoric elements constituted by three hydrophobic moieties that mimic the key residues of p53 (Phe19, Trp23, and Leu26).<sup>46</sup> Among the classes of small molecule inhibitors, spiro-oxindole derivatives (**1**) represent the most interesting compounds, being endowed with good potency and selectivity at disrupting p53–MDM2 interaction as well as possessing good oral bioavailability and pharmacokinetic (PK) properties.<sup>47–50</sup>

The disclosure of small molecule inhibitors of p53–MDM2 interaction, however, combines with very few quantitative structure–activity relationship studies (QSAR) of MDM2 inhibitors.<sup>51,52</sup>

Beside the use of ligand docking, pharmacophore modeling, and similarity-based methods,<sup>53–55</sup> QSAR studies are pivotal to enable the prioritization of analogues resulting from iterative virtual screening and thus the design of focused small molecule libraries around active ligands.<sup>56</sup>

\* Corresponding author. Telephone: +39 075 585 5160. Fax: +39 075 585 5114. E-mail: antonio@chimfarm.unipg.it.

<sup>†</sup> Dipartimento di Chimica e Tecnologia del Farmaco, Università di Perugia.

<sup>‡</sup> Siena Biotech S.p.A.

<sup>§</sup> Molecular Discovery Ltd.

<sup>||</sup> Laboratory for Chemometrics and Cheminformatics, Department of Chemistry, Università di Perugia.

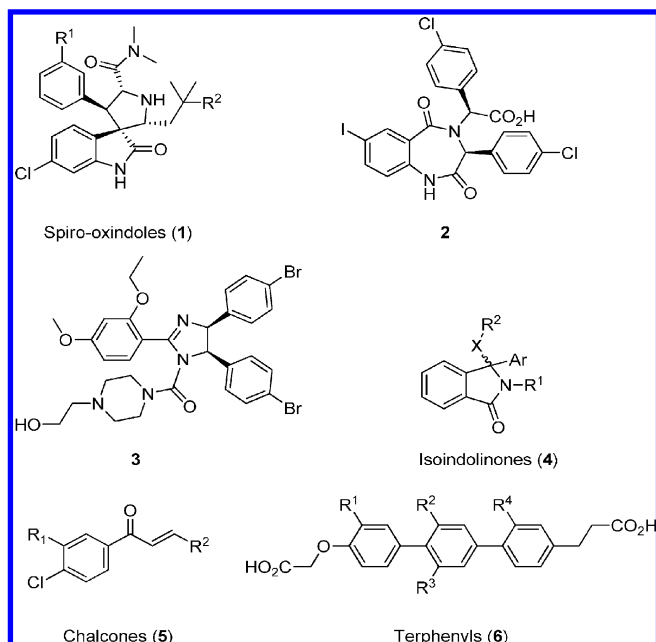


**Figure 1.** Chemical structures of some MDM2 inhibitors.

Furthermore, being mostly ligand-based approaches, their results may provide additional clues toward the pharmacophoric elements driving the molecular recognition of MDM2 inhibitors that complement those arising from the aforementioned structure-based studies. In this scenario, three-dimensional (3D)-QSAR approaches based on the description of small molecules in terms of molecular interaction fields (MIFs) are particularly relevant.<sup>57</sup> MIFs are able not only to generate predictive models of target affinity but also to disclose additional elements of interaction that may be hidden from first glance inspections of inhibitor-bound MDM2 structures.

As a consequence, in this work we deemed it of interest to construct a 3D-QSAR model of MDM2 inhibitors using molecular interaction fields calculated over a training set of 41 compounds. The model is endowed with good regression ( $R^2$ ) and crossvalidated ( $R_{XV}^2$ ) coefficients as well as predictive performance, as demonstrated by the 75% rate of correct predictions of an external test set of 36 compounds. In agreement with the experimental observations,<sup>16,17,21,26</sup> the inspection of the 3D-QSAR equation first reveals pivotal interaction points around the three hydrophobic moieties of the small molecule inhibitors that mimic the key p53 residues. Furthermore, the model shows the presence of additional interaction points in the part of the molecule that is on top of the canonical three hydrophobic groups. This observation is discussed in light of the current knowledge regarding the binding strategy of small molecule inhibitors to MDM2.

## METHODS

Models of small molecule inhibitors (Tables 1–3) were constructed with the program LigPrep v. 2.3, as implemented in the software package Schrödinger suite 2009.<sup>58</sup>

During this stage, all the possible configurations and tautomeric forms of isoindolinones were generated, and as a result, each compound yielded different molecular structures. Where present in the data set, the acidic groups were considered in their protonated form, and as a consequence,

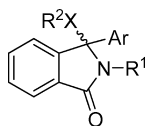
all molecules were endowed with a formal charge of 0. We deemed appropriate to adopt this approximation in the study to avoid any overestimation of the electrostatic component of the interaction. The resulting structures were submitted to energy refinement using the OPLS 2005 force field, a gradient convergence threshold of 0.05, and the implicit consideration of the water solvent. Atomic charges were calculated using the atomic charge parameters as implemented in the OPLS 2005 force field.<sup>59</sup>

In order to select one structure for the isoindolinone derivatives (7–64) out of the possible configurations and tautomers, all structures were compared to the bioactive configuration (*S, S*) and conformation of the benzodiazepine inhibitor (2) and Nutlin-2 (3) as observed in the MDM2 structures (pdb codes: 1T4E and 1RV1).<sup>17,26</sup> The comparison was carried out through the calculation of a similarity score based on the alignment between the query structure and the benzodiazepine inhibitor (2) or 3. This score, in particular, was calculated using Surflex v. 2.1 set with the option that attempts to optimize the alignment by lowering the root-mean-square deviation (rmsd) of superposition.<sup>60</sup> As a result, only the configuration and the tautomeric structure yielding the best similarity score with the benzodiazepine inhibitor (2) and/or 3 was selected for each isoindolinone and used for the following calculations. After this stage, the data set consisted in 79 compounds, including chalcones, terphenyls, and unique configurations and tautomers of isoindolinones. In order to fit the activity data in a positive range of values, the relative  $IC_{50}$  of the compounds in the data set was expressed as  $pIC_{50} = 6 - \log(IC_{50})$ .

The data set was submitted to two alternative strategies for the generation of a molecular alignment: a ligand-based MIF strategy using FLAP<sup>56</sup> and a structure-based docking strategy. FLAP analyzes the space around the ligand by using MIFs obtained by running a number of chemical probes (H, DRY, N1, O). The probes enable the identification of energetically favorable and unfavorable interactions. This information is used to align the ligand onto a template compound by superimposing energetically favorable and unfavorable interactions.

For each compound, up to 25 conformers were generated using a rmsd cutoff of 0.3 Å. MIFs were then calculated for each of the resulting conformations using the acceptor (O), donor (N1), hydrophobic (DRY), and shape (H) probes as implemented in FLAP and using a grid resolution of 0.75 Å. Finally, the conformations of the molecules were superimposed onto template compounds and scored on the basis of their fitness as resulting from the alignments of the MIFs. Three template compounds, in particular, were used as obtained by superimposing the crystal complexes of MDM2 with p53 (pdb code: 1T4F)<sup>17</sup> and Nutlin-2 (3, pdb code: 1RV1)<sup>26</sup> as well as benzodiazepine inhibitor (2, pdb code: 1T4E)<sup>17</sup> and by extracting the resulting aligned bioactive conformations of the ligands. While p53 was used as a potential template for aligning terphenyls and chalcones, Nutlin-2 (3) and the benzodiazepine inhibitor (2) were selected for superimposing isoindolinone derivatives. For each compound, the conformation yielding the best global score of MIF alignment was selected for the next steps of calculations.

The structure-based docking strategy was carried out using docking calculations on the data set with the GOLD

**Table 1.** Chemical Structures and Activity Values of Isoindolinone Derivatives

Compound	Training set	Test set	Ar	-R <sup>1</sup>	-XR <sup>2</sup>	pIC <sub>50</sub>
7	X		-Ph	-nPr		3.3
8	X		-Ph			3.36
9		X		-nPr		4.57
10	X		-Ph			3.38
11		X	-Ph			4.24
12		X	-Ph			3.94
13	X		-Ph			4.04
14		X	-Ph			3.61
15	X		-Ph			4.07
16		X	-Ph			3.64
17	X		-Ph			4.15
18		X	-Ph			3.49
19	X			-nPr		3.73
20		X	-Ph			3.56
21	X		-Ph			3.31
22		X				3.54
23	X		-Ph			3.46
24		X				4.13

Table 1. Continued

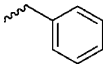
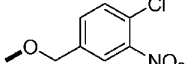
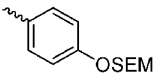
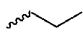
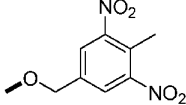
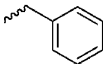
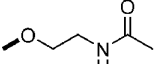
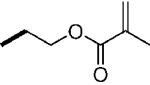
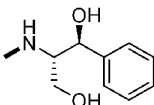
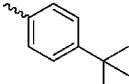
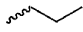
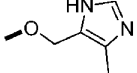
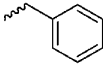
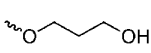
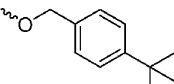
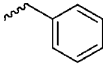
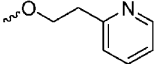
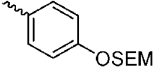
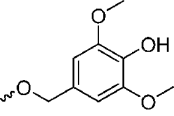
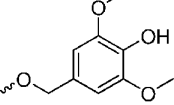
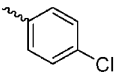
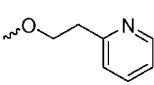
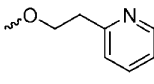
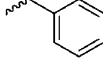
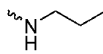
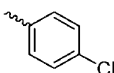
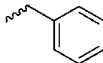
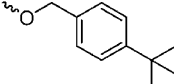
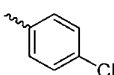
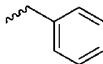
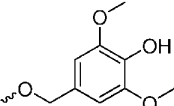
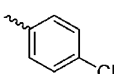
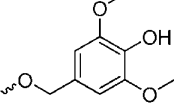
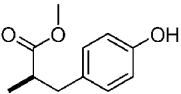
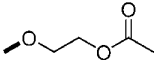
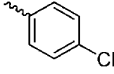
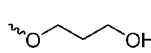
Compound	Training set	Test set	Ar	-R <sup>1</sup>	-XR <sup>2</sup>	pIC <sub>50</sub>
25	X		-Ph			3.69
26		X				3.99
27	X		-Ph			3.55
28		X	-Ph			3.99
29	X					4.19
30		X	-Ph			3.61
31	X		-Ph	-nPr		3.30
32		X	-Ph			3.69
33	X			-nPr		3.93
34		X	-Ph	-nPr		4.09
35	X			-nPr		4.24
36		X	-Ph	-nPr		4.00
37	X		-Ph			3.70
38		X				4.00
39	X					4.37
40		X		-nPr		5.28
41	X		-Ph			3.42
42		X		-nPr		4.79

Table 1. Continued

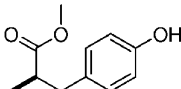
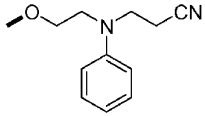
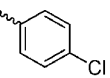
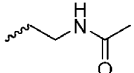
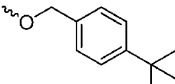
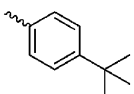
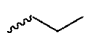
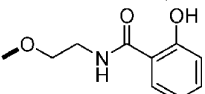
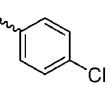
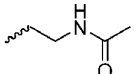
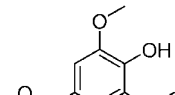
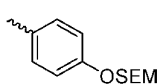
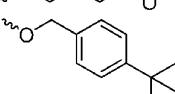
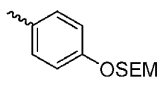
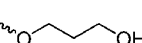
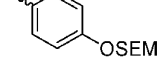
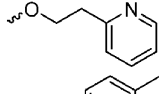
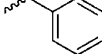
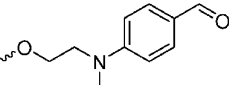
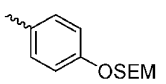
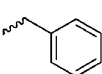
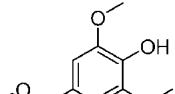
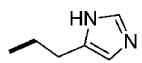
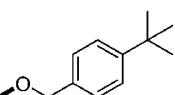
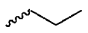
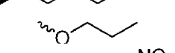
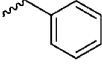
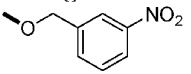
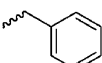
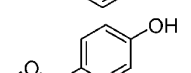
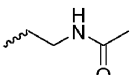
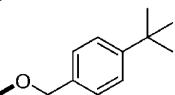
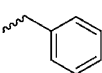
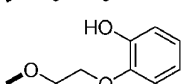
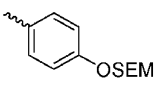
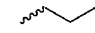
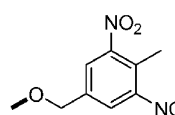
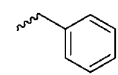
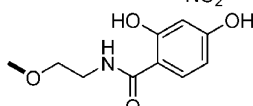
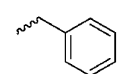
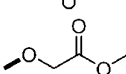
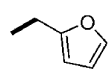
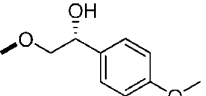
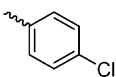
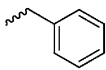
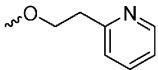
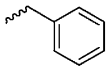
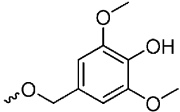
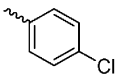
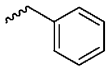
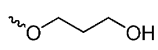
Compound	Training set	Test set	Ar	-R <sup>1</sup>	-XR <sup>2</sup>	pIC <sub>50</sub>
43	X		-Ph			4.06
44		X				4.04
45	X					4.15
46		X				4.12
47		X		-nPr		3.33
48		X		-nPr		3.32
49		X		-nPr		3.51
50	X		-Ph			3.72
51		X				3.59
52	X		-Ph			3.67
53	X		-Ph			3.70
54	X		-Ph			3.55
55	X		-Ph			4.10
56	X		-Ph			4.84
57	X		-Ph			3.66
58		X				3.99
59	X		-Ph			4.02
60	X		-Ph			3.30
61	X		-Ph			3.74

Table 1. Continued

Compound	Training set	Test set	Ar	-R <sup>1</sup>	-XR <sup>2</sup>	pIC <sub>50</sub>
62	X					4.58
63	X		-Ph			4.75
64	X					4.80

software.<sup>61</sup> Ligands were docked within the p53 binding site of MDM2, using the crystal structure of human MDM2 in complex with the small molecule inhibitor Nutlin-2 (**3**, pdb code: 1RV1).<sup>26</sup> The binding site was defined by hydrophobic fitting points calculated on the target for an 8 Å radius around the cocrystallized ligand. GoldScore was used as fitness function, while default genetic algorithm parameter settings were applied. Thirty poses were generated for each ligand, being early termination allowed when the top 10 solutions were within 1.5 Å rmsd. The best scoring pose was selected for each ligand and used as an input structure for subsequent 3D-QSAR analysis.

At this regard, we deemed advisable to avoid any further refinement of the docking poses or whole protein–inhibitor complexes, beyond those operated by Gold, in order to keep a constant reference system in terms of energy and scoring functions. According to the MIF and docking alignments, the aligned molecules were instrumental to calculate two different enveloping van der Waals surfaces constituting 7954 and 7984 interaction points, respectively. For each of these points, the interactions between each compound and hydrophobic (DRY) and hydrophilic (H<sub>2</sub>O) probes were calculated using the GRID program.<sup>62</sup> The resulting interaction values were used as independent variables to perform a genetic function approximation study (GFA).<sup>63</sup> The MIF- and the docked-data sets were equally split into a training set of 41 compounds and a test set of 36 small molecules. This was first accomplished generating two random data samples of 41 and 36 objects from the distribution of activity values. Then, the data samples were manually edited in order to have a high degree of chemical diversity in both training and test set compounds (training set composition: 34 isoindolinone derivatives, 3 chalcones, and 4 terphenyls; test set: 24 isoindolinone derivatives, 2 chalcones, and 10 terphenyls). The resulting data samples have similar ranges of activity values as evidenced by the averages and standard deviations (pIC<sub>50</sub> average ± standard deviation for the data, training, and test sets was 3.98 ± 0.53, 3.97 ± 0.51, and 3.99 ± 0.55, respectively).

The following were the settings used in the GFA study: number of final models 10, initial equation length 1, maximum equation length 10, population size 100, maximum number of generation 100, and lack-of-fit (LOF) smoothness parameter 0.5.

Leave-one-out cross-validation protocols were used to determine the statistical significance of the resulting 3D-QSAR equations. The predictive index of the generated models was given by the crossvalidated  $R_{XV}^2$  (or  $q^2$ ). Correct predictions were defined as those showing an absolute value

of residual of prediction (difference between predicted and experimental pIC<sub>50</sub>) lower than 1. Interestingly, no correlation was observed between the number of torsional angles in the molecules of the training set and the residual of predictions (see Supporting Information, Figures s1–s3), suggesting that the extend of conformational sampling should not affect the results of the study. The statistical analyses were performed in Discovery Studio using the default settings.<sup>64</sup>

## RESULTS

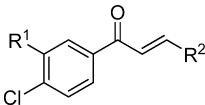
**Data Set.** Although different classes of small molecule inhibitors of p53–MDM2 interaction are reported in literature,<sup>40,41</sup> the use of heterogeneous biological assays to assess their activity restricts the construction of a large data set of molecules to a few classes with homogeneous data. Consequently, we have collected a set of MDM2 inhibitors tested in ELISA assays,<sup>65–67</sup> as they span a wide range of activities. The data set, in particular, includes 58 isoindolinone derivatives (**7–64**, Table 1), 5 chalcones (**65–69**, Table 2), and 14 terphenyls (**70–83**, Table 3) that were selected in order to get a normal distribution of activity values while keeping a high degree of chemical diversity.

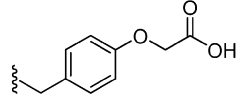
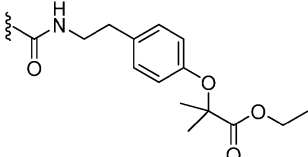
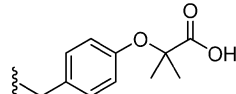
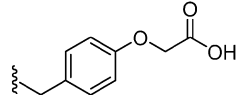
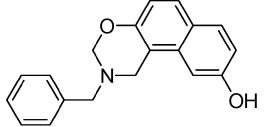
Remarkably, the chemical diversity of our data set reflects the use of different strategies to design MDM2 inhibitors. In particular, while chalcones (**65–69**) and terphenyls (**70–83**) were developed as mimetic of the p53 α helix, isoindolinone derivatives (**7–64**) were designed with the application of structure-based approaches.

Since the configuration of active isoindolinone derivatives is undefined,<sup>65</sup> multiple configurations and tautomeric structures were generated for this class of molecules. Then, a unique structure for each isoindolinone derivative was selected on the basis of a similarity score calculated over the bioactive configuration (*S, S*) and conformation of the benzodiazepine inhibitor (**2**) and Nutlin-2 (**3**), as observed in the relative experimental MDM2 structures (pdb codes: 1T4E and 1RV1).<sup>17,26</sup> Further details concerning the selection of the more likely bioactive configuration, conformation, and tautomer of isoindolinones are reported in the Methods Section.

**Molecular Alignment.** Two alternative strategies were adopted for the generation of a molecular alignment: (i) a ligand-based MIF strategy (Figure 2a) and (ii) a structure-based docking strategy (Figure 2b). This was motivated by the inefficacy of docking experiments to accurately predict a unique binding mode for isoindolinones as well as for other small molecule inhibitors of MDM2.<sup>65</sup> Accordingly, we



**Table 2.** Chemical Structures and Activity Values of Chalcones


Compound	Training set	Test set	-R <sup>1</sup>	-R <sup>2</sup>	pIC <sub>50</sub>
65		X	H		3.69
66	X		H		3.60
67		X	H		3.60
68	X		Cl		4.31
69	X				3.60

deemed it of interest to comparatively investigate 3D-QSAR models generated starting from ligand- and structure-based strategies. Indeed, while the latter was proven successful in many studies of more 'conventional' biological targets,<sup>68,69</sup> it is still arguable whether it may also prove good in cases of protein-protein interaction targets that involve transient hollow binding sites.<sup>70</sup>

For the ligand-based MIF strategy, we used FLAP<sup>71</sup> to superimpose the data set of compounds onto three aligned template structures: p53, Nutlin-2 (**3**), and a benzodiazepine inhibitor (**2**). The alignment of the template structures, in particular, was obtained by superimposing the crystal complexes of MDM2 with p53 (pdb code: 1T4F)<sup>17</sup> and Nutlin-2 (**3**, pdb code: 1RV1)<sup>26</sup> as well as the benzodiazepine inhibitor (**2**, pdb code: 1T4E)<sup>17</sup> and by extracting the resulting aligned bioactive conformations of the ligands. Then, p53 was used as a potential template to superimpose terphenyls and chalcones, whereas Nutlin-2 (**3**) and the benzodiazepine inhibitor (**2**) were instrumental to align the isoindolinone derivatives. For each compound of the data set, the conformation yielding the best global score of MIF alignment was stored and used for the next steps of calculations. From here onward, we will refer to this data set of aligned compounds as the 'MIF-data set'.

Concerning the structure-based docking strategy, the data set of compounds was docked into the crystal structure of MDM2 bound to **3** (pdb code: 1RV1),<sup>26</sup> and only the best scoring pose was saved for each of the molecules. From here onward, we will refer to the data set of compounds aligned by this strategy as the 'docked-data set'.

**3D-QSAR Models.** Following the alignment protocols, the aligned MIF- and docked-data sets were used to generate two different enveloping van der Waals surfaces constituting of 7954 and 7984 interaction points (Figure 2c and d), respectively. We deemed this computational approach as

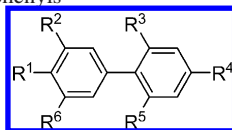
suitable to increase the probability of identify the interaction points closely located on the contact surfaces between the ligand and the binding site, while avoiding the generation of grid-based interaction points that, being located far from those surfaces, could add noise to the statistical analysis.

As an additional consideration, the interaction points mapped on the enveloping van der Waals surfaces could avoid the artifacts introduced using regularly spaced grids for the placement of probes and interaction energies.

The energetic values at the surface points were calculated using the hydrophobic (DRY) and hydrophilic (H<sub>2</sub>O) probes as implemented in the program GRID.<sup>62</sup> As a result, two molecular interaction fields were generated and filtered to remove the interaction points with the lowest variance. After the filtering procedure, the interaction point energies were defined as independent variables, while the activity of the inhibitors, expressed as pIC<sub>50</sub>, was set as the dependent variable. Then, the MIF- and the docked-data sets were equally split into a training set of 41 compounds and a test set of 36 small molecules. This was accomplished trying to keep a similar distribution of activity values and high degree of chemical diversity in both training and test set compounds (see Method Section for further details).

The two training sets were used to construct 3D-QSAR models using a GFA.<sup>63</sup> The GFA provides the Friedman's LOF score, an estimation of the error that penalizes models with too many independent variables.<sup>72</sup>

The final best five 3D-QSAR models resulting from the MIF- and docked-training sets are reported in Table 4, respectively. From the inspection of the results, it is clear that the ligand-based MIF strategy outperformed the structure-based docking strategy, with the average regression ( $R^2$ ) and crossvalidated ( $R_{XV}^2$ ) coefficients  $\pm$  standard deviation being  $0.835 \pm 0.02$  and  $0.749 \pm 0.02$  for the former and  $0.632 \pm 0.03$  and  $0.480 \pm 0.03$  for the latter. Consequently, we

**Table 3.** Chemical Structures and Activity Values of Terphenyls

Comp.	Training set	Test set	-R <sup>1</sup>	-R <sup>2</sup>	-R <sup>3</sup>	-R <sup>4</sup>	-R <sup>5</sup>	-R <sup>6</sup>	pIC <sub>50</sub>
70	X		-iBu					-H	4.82
71	X		-Bn					-H	4.70
72	X		-Bn					-H	4.92
73		X		-iBu	-Bn		-H	-H	3.89
74		X	-H	-iPr			-H	-H	3.82
75		X	-H	-iPr	-iBu		-H	-H	5.00
76		X					-H		3.35
78		X		-iBu			-H	-H	5.00
79		X		-iBn				-H	5.00
80		X						-H	4.82
81		X		-iBu				-H	4.92
82		X						-H	4.70
83		X		-Bn				-H	3.35



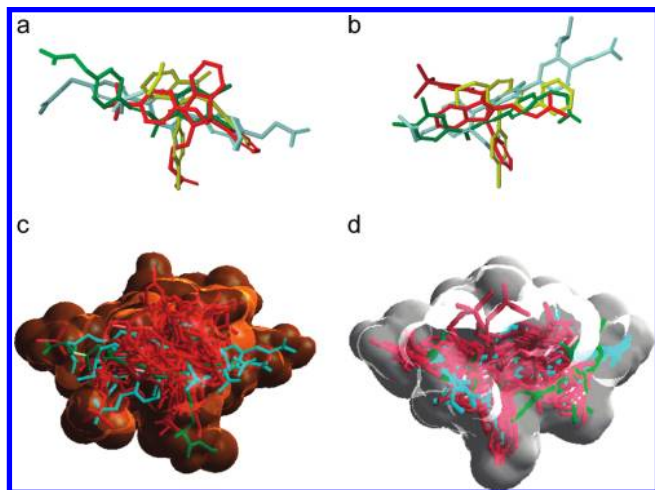


**Figure 2.** Comparison between the alignments generated using the MIF strategy (a) and the docking strategy (b). For clarity, only the most active compounds **56** (yellow sticks), **64** (red sticks), **68** (green sticks) and **81** (cyan sticks) are shown. van der Waals surfaces enveloping the training set compounds aligned according to the MIF strategy (c) or structure-based docking strategy (d).

decided to analyze only the 3D-QSAR models resulting from the MIF-training set.

Analysis of the independent variables selected in the five models (Table 5) reveals that the equations contain six or seven terms. Three of them are constantly present in the equations: DRY-1, DRY-2, and DRY-3 (average coefficient  $\pm$  standard deviation =  $0.139 \pm 0.012$ ,  $0.127 \pm 0.006$ , and  $0.094 \pm 0.003$ , respectively). Two additional ones, namely DRY-4 and DRY-5 (average coefficient  $\pm$  standard deviation =  $0.141 \pm 0.004$  and  $0.098 \pm 0.001$ , respectively), are

present in four of the five equations. The remaining terms slightly change their Cartesian coordinates around the inhibitors: DRY-6 and DRY-7 (average coefficient  $\pm$  standard deviation =  $0.062 \pm 0.006$  and  $0.074 \pm 0.009$ , respectively). Since the information contained in the five models is almost the same, MIF-models 1, 4, and 5 were further analyzed insofar as showing the highest regression ( $R^2$ ) and crossvalidated ( $R_{\text{cv}}^2$ ) coefficients. Figure 3 shows the plot of experimental versus predicted  $\text{pIC}_{50}$  for the molecules of the training set according to MIF-model 1, 4, and 5. The variables composing the equations of MIF-models 1, 4, and 5 are largely independent, as  $R^2=0.423$  is the largest intercorrelation observed for DRY-1 and DRY-6 (see Supporting Information, Tables s1–s3). Additional statistical parameters of MIF-models 1, 4, and 5 are reported in the Supporting Information (see Tables s4–s6). The statistical meaning of MIF-models 1, 4, and 5 was also assessed by scrambling randomly the activity data of the training set in each model for 10 runs (see Supporting Information, Table s7). As a result, the highest  $R^2$  found was 0.339 in MIF-model 1, pinpointing a good statistical significance of the models. The predictive power of these models was appraised using an external test set of 36 compounds taken from the MIF-data set (Figure 4). The analysis of residuals (Figure 4) shows that 9 out of 36 compounds are not optimally predicted in MIF-models 1 and 4 (Figure 4a and b): isoindolinones **34**, **40**, **42**, and **47**, and terphenyls **75**, **78–80**, and **83**. Ten outliers are found in MIF-model 5: isoindolinones **34**, **38**, **40**, **42**, and **47** and terphenyls **75**, **76**, **78**, **80**, and **83** (Figure 4c). As a consequence, while 72% of the external test set yielded satisfactory predictions in MIF-model

**Table 4.** Top Five 3D-QSAR Models Resulting from the Structure-Based Docking and Ligand-Based MIF Strategies<sup>a</sup>

model	$R^2$	$R_{\text{cv}}^2$	rms residual error	Friedman LOF <sup>b</sup>	adj. $p$ -value <sup>c</sup>
docked-model 1	0.625	0.476	0.348	0.215	$1.10 \times 10^4$
docked-model 2	0.620	0.469	0.350	0.218	$1.38 \times 10^4$
docked-model 3	0.619	0.460	0.351	0.219	$1.48 \times 10^4$
docked-model 4	0.616	0.463	0.352	0.220	$1.64 \times 10^4$
docked-model 5	0.681	0.533	0.326	0.221	$3.13 \times 10^5$
MIF-model 1	0.850	0.762	0.216	0.117	$7.87 \times 10^{10}$
MIF-model 2	0.815	0.725	0.237	0.117	$4.17 \times 10^9$
MIF-model 3	0.815	0.723	0.237	0.117	$4.26 \times 10^9$
MIF-model 4	0.849	0.761	0.217	0.117	$8.34 \times 10^{10}$
MIF-model 5	0.849	0.772	0.217	0.117	$8.47 \times 10^{10}$

<sup>a</sup> Docked-model 1–5 and MIF-model 1–5. <sup>b</sup> The LOF score is an estimation of the error that penalizes models with too many independent variables. <sup>c</sup> Adjusted  $p$ -value by applying Bonferroni correction.

**Table 5.** Interaction Points Selected as Independent Variables of the MIF-Models along with the Relative Coefficients and Cartesian Coordinates

variable	(x; y; z)	MIF-model 1	MIF-model 2	MIF-model 3	MIF-model 4	MIF-model 5
constant	—	3.977	3.970	3.973	3.973	4.026
DRY-1	26.81; -21.32; -1.69	0.128	0.152	0.151	0.127	0.135
DRY-2	36.87; -19.82; -8.35	0.123	0.134	0.133	0.119	0.073
DRY-3	29.81; -27.32; -12.85	0.093	0.097	0.096	0.091	0.091
DRY-4	22.81; -19.88; -12.35	0.139	—	0.147	0.140	0.138
DRY-5	25.55; -18.82; -3.85	0.097	0.097	0.098	0.098	—
DRY-6	26.31; -26.03; 0.15	0.058	—	—	0.059	0.069
DRY-7	36.81; -27.32; -11.08	0.064	0.079	0.078	—	—
DRY-8	22.81; -19.82; -12.31	—	0.145	—	—	—
DRY-9	36.81; -27.32; -11.45	—	—	—	0.063	—
DRY-10	26.04; -18.82; -3.35	—	—	—	—	0.140
DRY-11	37.31; -25.82; -12.00	—	—	—	—	0.073

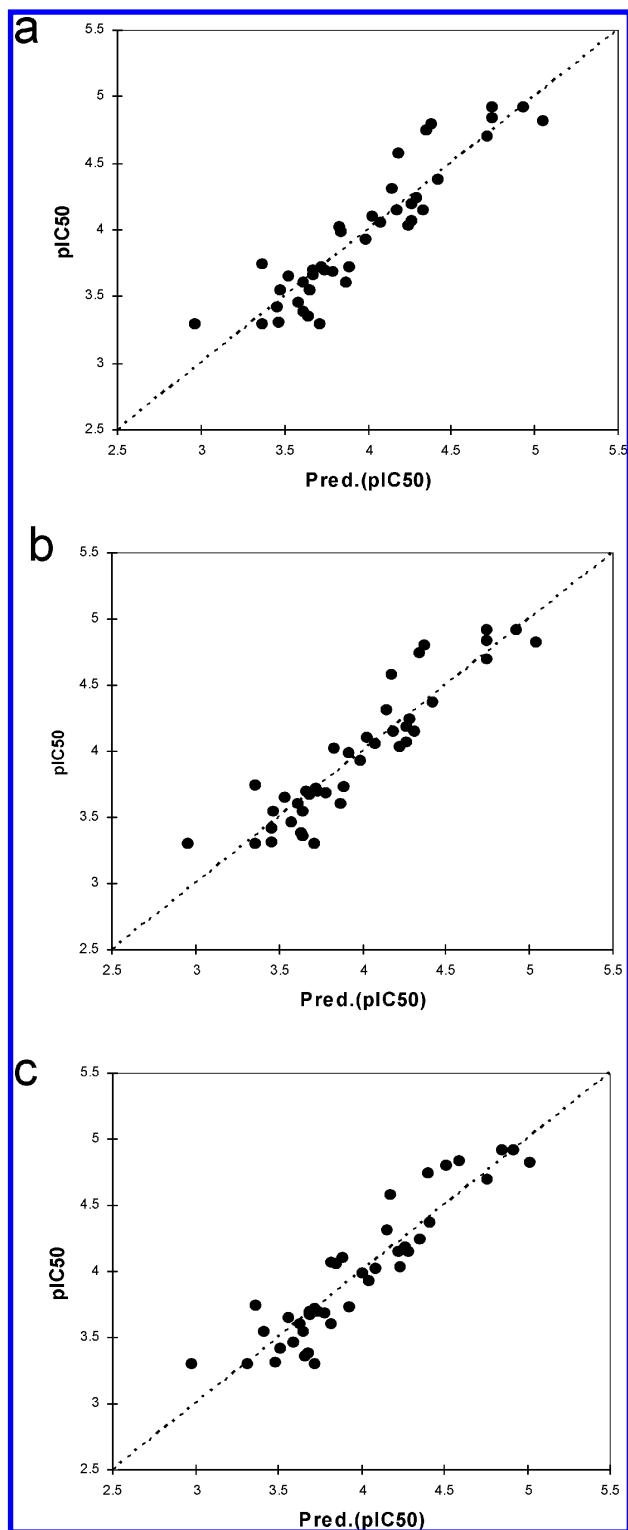


**Figure 3.** (a) Plot of experimental versus predicted  $pIC_{50}$  for the molecules of the training set according to MIF-model 1. (b) Plot of experimental versus predicted  $pIC_{50}$  for the molecules of the training set according to MIF-model 4. (c) Plot of experimental versus predicted  $pIC_{50}$  for the molecules of the training set according to MIF-model 5.

5, 75% of the external test set was correctly predicted in MIF-models 1 and 4.

As an additional analysis, we addressed whether MIF-models tend to explain interfamily differences among isoindolinones, chalcones, and terphenyls, rather than intrafamily differences. This was achieved by developing an additional

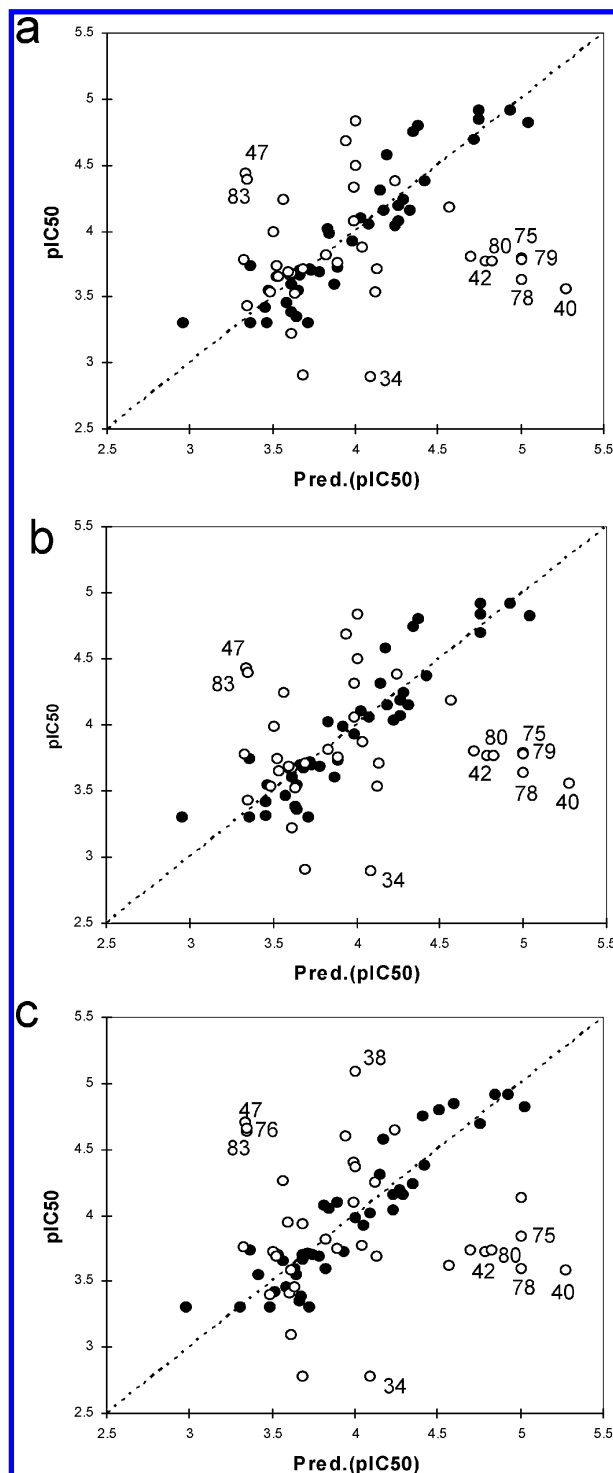


**Figure 4.** (a) Plot of experimental versus predicted  $pIC_{50}$  for the molecules of the test set according to MIF-model 1. (b) Plot of experimental versus predicted  $pIC_{50}$  for the molecules of the test set according to MIF-model 4. (c) Plot of experimental versus predicted  $pIC_{50}$  for the molecules of the test set according to MIF-model 5. Compounds with absolute residual values higher than 1 are defined as outliers and labeled.

3D-QSAR model on the isoindolinone derivatives of the training set (Figure 5, Table 6). The results show a statistical meaningful model ( $R^2 = 0.761$ ;  $R_{XV}^2 = 0.708$ ) that leads to similar findings. In particular, the inspection of the 3D-QSAR equation reveals the presence of six terms that are also found in MIF-models developed using the whole training set (Table 6). When applied to predict the activity of isoindolinones

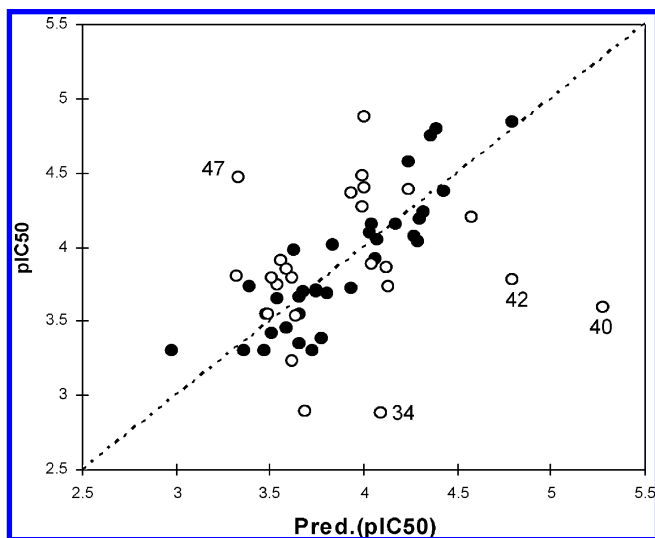


**Figure 5.** Plot of experimental versus predicted  $pIC_{50}$  for the isoindolinone derivatives of the training and test sets according to a local 3D-QSAR model.

**Table 6.** Interaction Points, Coefficients and Cartesian Coordinates of the Local Model Generated Using Only the Isoindolinones of the Training Set

variable	(x; y; z)	local-model
constant	—	3.991
DRY-1	26.81; -21.32; -1.69	0.131
DRY-2	36.87; -19.82; -8.35	0.130
DRY-3	29.81; -27.32; -12.85	0.100
DRY-4	22.81; -19.88; -12.35	0.139
DRY-5	25.55; -18.82; -3.85	0.095
DRY-6	26.31; -26.03; 0.15	0.062

belonging to the external test set, the model found four outliers (**34**, **40**, **42**, and **47**, Figure 5) that are also present as outliers in the predictions of MIF-models 1, 4, and 5.

## DISCUSSION

In this work we have developed 3D-QSAR models of p53-MDM2 inhibitors adopting two alternative approaches to align compounds according to either their molecular fields of interaction (MIF) or their binding pose as resulting from docking experiments.

Comparatively, the top five 3D-QSAR models resulting from the ligand-based MIF strategy have shown better regression ( $R^2$ ) and crossvalidated ( $R_{XV}^2$ ) coefficients than the relative 3D-QSAR models arising from structure-based docking strategy (Table 4). Considering MIF-model 1 as the reference model, inspection of its equation has revealed seven independent variables that encode as many interaction points within the binding cleft of MDM2 (Table 5). In agreement with our previous results,<sup>27,29</sup> all of these points encode hydrophobic interactions (DRY probe), pinpointing that this is the driving force of ligand binding to MDM2. Three interaction points are constantly present in all of the five MIF-based models (DRY-1, DRY-2, and DRY-3), though two additional ones slightly change their location around the inhibitors depending on the MIF-model (DRY-6 and DRY-7). Finally, DRY-4 and DRY-5, are present in four of the five equations. As far as the coefficients are concerned, DRY-1, DRY-2, and DRY-4 show the highest values in the equation of MIF-model 1.

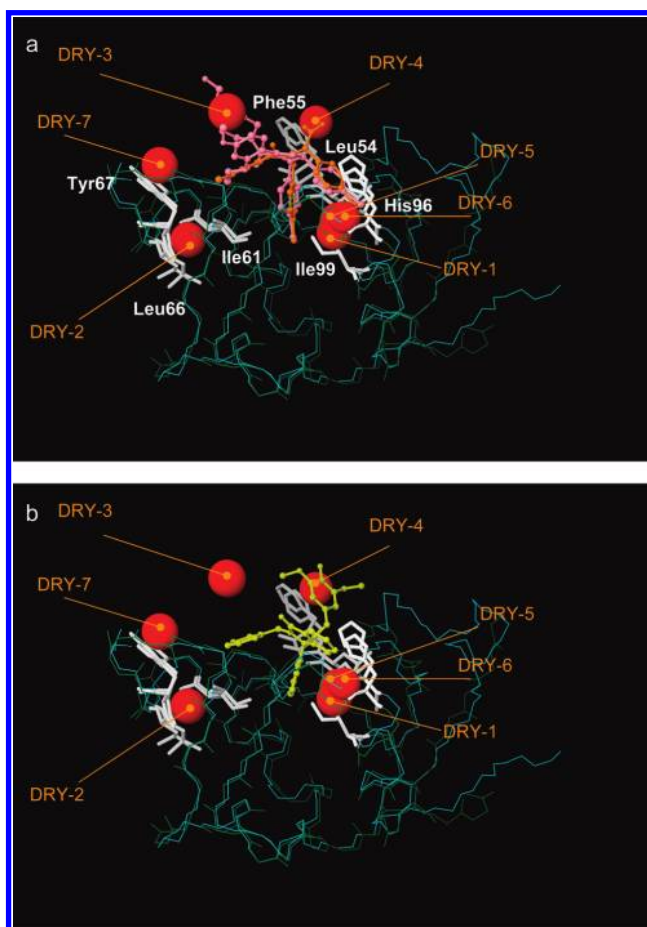


**Figure 6.** (a) Plot of the interaction points of MIF-model 1 into the experimental structures of MDM2 in complex with the benzodiazepine inhibitor (**2**, pdb code: 1T4E) and Nutlin-2 (**3**, pdb code: 1RV1); **2** is colored as orange, **3** is colored as pink, interaction points are shown as red balls and labeled, and residues close to the interaction points are colored as white and labeled. (b) Compound **63** placed into the p53 binding cleft of MDM2 (pdb codes: 1T4E and 1RV1) according to the MIF alignment over the benzodiazepine inhibitor (**2**) and Nutlin-2 (**3**).

Interestingly, these results are in agreement with those obtained with the generation of a local model on the isoindolinone derivatives of the training set (Figure 5, Table 6). Overall, this observation suggests that MIF-models are not biased toward the explanation of the interfamily differences of the training set, but they are also able to explain intrafamily differences. At this concern, however, we cannot rule out that this is due to the composition of the training set used to generate the MIF-models that counts the 83% rate of isoindolinone derivatives. The projection of the interaction points of MIF-model 1 onto some experimental structures of MDM2 (pdb code: 1RV1, 1T4E, 1TTV, and 1Z1M) provides some structural basis to the quantitative correlation and sheds further light on the process of ligand recognition by the oncogenic protein. As a result, a high degree of binding specificity is observed around the three hydrophobic moieties of the small molecule inhibitors that mimic the key p53 residues (Figures 6 and 7). Indeed, the most present and highly weighted interaction points DRY-1 (presence 5/5; average coefficient =  $0.139 \pm 0.012$ ) and DRY-2 (presence 5/5; average coefficient =  $0.127 \pm 0.006$ ) are placed within the canonical p53 binding cleft, being located near Ile61, Leu66, and Ile99, respectively. In addition, DRY-5 (presence 4/5; average coefficient =  $0.098 \pm 0.001$ )

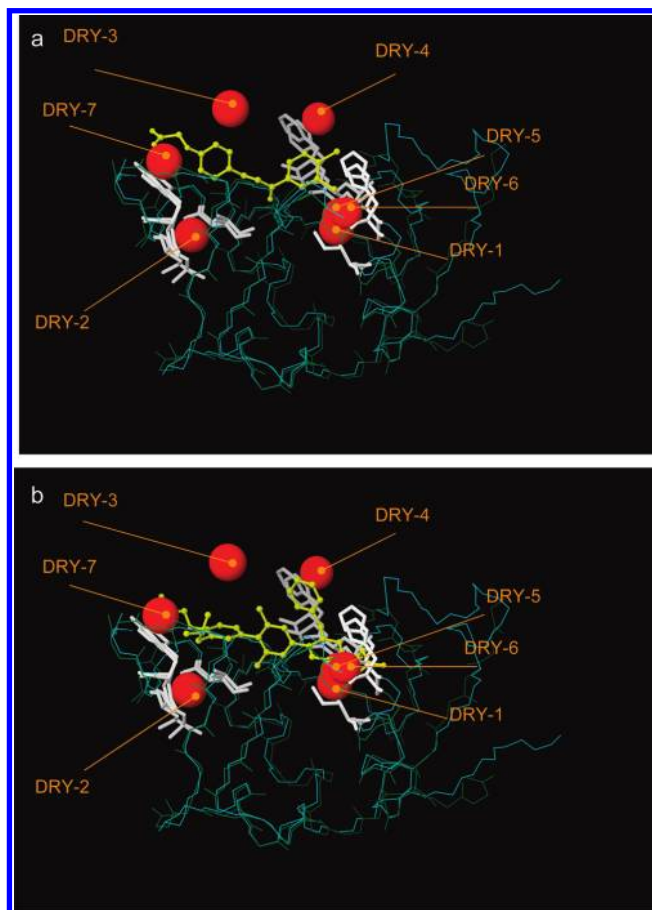


**Figure 7.** (a) Compound **68** placed into the p53 binding cleft of MDM2 (pdb codes: 1T4E and 1RV1) according to the MIF alignment over p53. (b) Compound **70** placed into the p53 binding cleft of MDM2 (pdb codes: 1T4E and 1RV1) according to the MIF alignment over p53.

is also located in this pocket, being close to the side chain of Leu54. Conversely, DRY-4 (presence 4/5; average coefficient =  $0.141 \pm 0.004$ ) is located on the surface of MDM2, being close to Phe55. As a consequence, this variable may encode a specific hydrophobic interaction between either terphenyls or the methoxy-substituted aromatic moiety of some of the most potent isoindolinone derivatives, such as compounds **39** and **63**, and the side chain of Phe55 (Figures 4b and 5b).

Analogously, the less important interaction points DRY-6 (presence 3/5; average coefficient =  $0.062 \pm 0.006$ ) and DRY-7 (presence 3/5; average coefficient =  $0.074 \pm 0.009$ ) are located close to the surface residues His96 and Tyr67 of MDM2, respectively.

It should be mentioned that these interaction points are also placed quite far away from the chemical scaffold of isoindolinones but close to the chemical scaffold of chalcones and terphenyls (Figure 5). Accordingly, they may specifically encode weak hydrophobic interactions of chalcones and terphenyls with the side chains of His96 and Tyr67.

Finally, the interaction point DRY-3 (presence 5/5; average coefficient =  $0.094 \pm 0.003$ ) is placed at the upper part of the inhibitors, completely exposed to the solvent (Figures 3 and 4). Although we are aware of the general risk of occurring fallacy with QSAR models,<sup>73</sup> we may put forward two hypotheses to interpret the meaning of DRY-3. In the first case, we may envisage that this interaction point is a

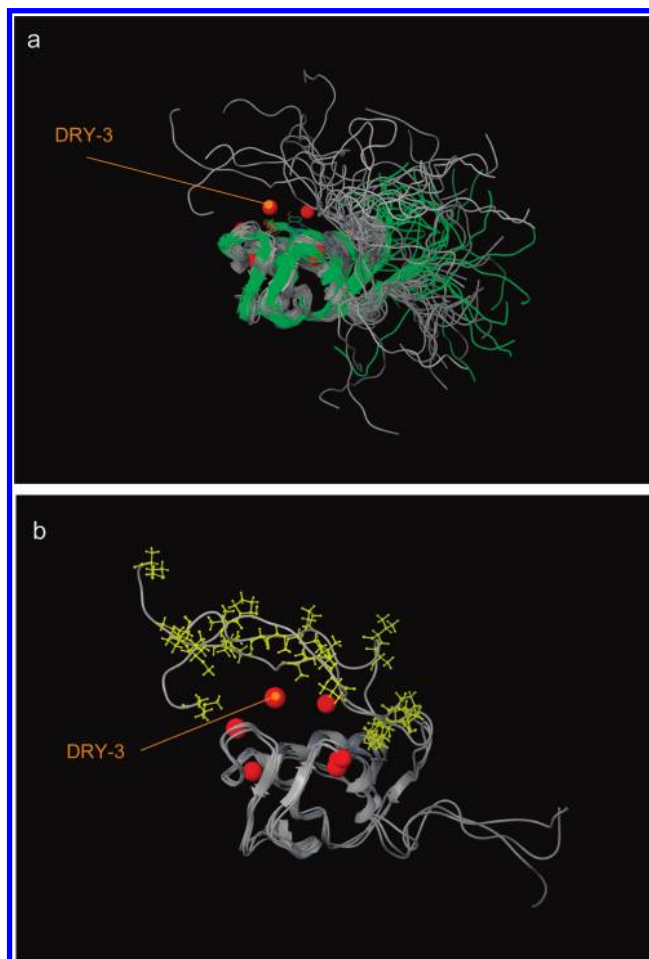


**Figure 8.** (a) Plot of the interaction points (red balls) of MIF-model 1 into the NMR unbound structure of MDM2 (pdb code: 1Z1M, gray ribbons) and into the NMR benzodiazepine-bound structure of MDM2 (pdb code: 1TTV, green ribbons). (b) Plot of the interaction points (red balls) of MIF-model 1 into selected frames of the NMR unbound structure of MDM2 (pdb code: 1Z1M) showing the bending of the N-terminal part over the p53 binding cleft.

noise variable arising from the intrinsic limitation of the study that wrongly takes into account the ligand–target interaction, as occurring around the entire molecular shape of the inhibitor and not, more correctly, along one of its faces. The relatively low coefficient of DRY-3 would sustain this scenario.

The second hypothesis is speculative and challenges the previous suggestion regarding the binding strategy of small molecule inhibitors to MDM2.<sup>16</sup> This suggestion, in particular, states that the upper part of small molecule inhibitors, such as the piperazine group of Nutlin-2 (**3**), produces no intermolecular interactions, being located beyond any contact with MDM2 and fully exposed to the solvent. This is based on the observation that in the NMR structure of MDM2 with a benzodiazepine inhibitor (pdb code: 1TTV), the N-terminal part of the oncogenic protein does not take part in ligand binding.<sup>16</sup> Conversely, the location of DRY-3 would underpin an active role of the N-terminal part of MDM2 in the process of ligand binding through its hydrophobic residues (Figure 8).

It should be mentioned that the aforementioned NMR structure (pdb code: 1TTV) is a truncated form of MDM2 (residues 13–119), being the apo-form of MDM2 (pdb code:



1Z1M), the only complete structure at the N-terminal part so far available (residues 1–119).<sup>18</sup> Although we cannot exclude that different classes and/or specific inhibitors of MDM2 may interact with the full N-terminal part of the oncogenic protein, in literature we could not find data reporting different activities of small molecule inhibitors depending on the truncated or full length form of MDM2, since different truncated forms of the protein have been used in diverse biological assays.

Nevertheless, as an important clue sustaining this hypothesis, very recently it has been reported that the N-terminal region of MDM2 has an active role in the regulation of the allosteric cross-talk between the p53 binding cleft and the central domain of MDM2, thereby promoting the E3 ubiquitin ligase function of the oncogenic protein.<sup>74</sup> According to that study, a phosphorylated form of the N-terminal part of MDM2 would interact with a charged surface pocket of MDM2 constituted of Arg97 and Lys98, thereby bending over the p53 binding cleft.

As a consequence, it is likely that the high flexibility of the N-terminal region of MDM2 may also promote conformational changes that produce intermolecular interactions with some chemotypes of small molecules docked into the p53 binding cleft. At this regard, it is worth mentioning that a more recent study reports the reduced thermostability of ligand-bound MDM2 following a lid-deleting mutation.<sup>75</sup> Thus, albeit pending for further experimental appraisals, the second hypothesis may provide intriguing clues on additional pharmacophoric elements that feature the molecular recognition of some MDM2 inhibitors.

Finally, for a practical assessment of the study, the predictivity of MIF-models 1, 4, and 5 was evaluated using an external test set of 36 compounds (Figure 4). As a result, MIF-models 1 and 4 yielded the best performance, being able to satisfactorily predict with 75% success the external test set of compounds. In both models, while seven compounds (**34**, **40**, **42**, **75**, **78**, **79**, and **80**) were predicted less active with respect to their IC<sub>50</sub>, two compounds (**4783**) were overpredicted. We cannot rule out that these poor predictions may arise from a limited sampling of the range of potencies in the training set or from the presence of unpredictable activity cliffs around the chemical scaffolds of isoindolinones and terphenyls.<sup>76</sup> However, this result is very encouraging in view of future applications of the study aimed at the prioritization of analogues of active ligands resulting from virtual screening and the design of focused small molecule libraries around known active inhibitors of MDM2.

## CONCLUSIONS

Recent years have seen a great deal of interest in developing small molecule inhibitors of p53-MDM2 interaction as potential novel anticancer agents. While these endeavors have been accompanied by attempts to investigate the molecular basis of ligand recognition in MDM2 through either experimental approaches, such as NMR and X-ray crystallography, or development of computational models, very few QSAR studies have hitherto been reported.

Here, we have developed the first 3D-QSAR models of MDM2 small molecule inhibitors with the use of molecular

interaction fields (MIF). While a ligand-based MIF strategy and a structure-based docking strategy were both instrumental to generate molecular alignments of the starting data set of compounds, only the ligand-based MIF strategy was able to provide satisfactory results in terms of better regression ( $R^2$ ) and crossvalidated ( $R_{XV}^2$ ) coefficients using a genetic function approximation (GFA) study for the 3D-QSAR model construction.

The interaction points of the final 3D-QSAR equations, while in agreement with the previously reported structure–activity relationship of MDM2 inhibitors, disclose pharmacophoric elements that feature the molecular recognition of small molecule inhibitors according to their relative chemical class. Beside the presence of important interaction points around the three hydrophobic moieties of the small molecule inhibitors that mimic the key p53 residues, the 3D-QSAR equations unveil some interaction points located on the surface of MDM2 that encode specific anchoring points of chalcones and terphenyls. Even more surprisingly, a hydrophobic interaction located on the upper part of small molecule inhibitors pinpoints an active role of the N-terminal part of MDM2 in the process of ligand binding. Overall, these results will be used to aid the design of novel potent inhibitors of p53-MDM2 interaction and to prioritize the synthesis of analogues of active ligands.

## ACKNOWLEDGMENT

This work was supported by the European Union. FP6 PRIORITY LSH-2005-2.2.0-8: Small-ligand libraries: improved tools for exploration and prospective antitumour therapy. DePPICT Project (**D**esigning **T**herapeutic **P**rotein-**P**rotein **I**nhibitors for **B**rain **C**ancer **T**reatments) Contract number: LSHC-CT-2007- 037834 (<http://www.deppict.eu/home.jsp>). Dr. Graeme Robertson (Siena Biotech S.p.A.) is gratefully acknowledged for thoughtful suggestions and comments during the preparation of the manuscript.

**Supporting Information Available:** Correlation matrix between the selected variables of MIF-model 1, 4, and 5. Standardized coefficients and additional statistical parameters for the selected variables of MIF-model 1, 4, and 5. (95% confidence interval). Results of the scrambling test on the training set of MIF-models 1, 4 and 5. Correlation between the number of torsional angles in the molecules of the training set (x axis) and the residual of predictions of MIF-model 1, 4, and 5 (y axis). This material is available free of charge via the Internet at <http://pubs.acs.org>.

## REFERENCES AND NOTES

- (1) Momand, J.; Wu, H. H.; Dasgupta, G. MDM2—master regulator of the p53 tumor suppressor protein. *Gene* **2000**, *242*, 15–29.
- (2) Arrowsmith, C. H.; Morin, P. New insights into p53 function from structural studies. *Oncogene* **1996**, *12*, 1379–1385.
- (3) Oliner, J. D.; Kinzler, K. W.; Meltzer, P. S.; George, D. L.; Vogelstein, B. Amplification of a gene encoding a p53-associated protein in human sarcomas. *Nature* **1992**, *358*, 80–83.
- (4) Marchetti, A.; Buttitta, F.; Pellegrini, S.; Merlo, G.; Chella, A.; Angeletti, C. A.; Bevilacqua, G. mdm2 gene amplification and overexpression in non-small cell lung carcinomas with accumulation of the p53 protein in the absence of p53 gene mutations. *Diagn. Mol. Pathol.* **1995**, *4*, 93–97.

- (5) Reifenger, G.; Liu, L.; Ichimura, K.; Schmidt, E. E.; Collins, V. P. Amplification and overexpression of the MDM2 gene in a subset of human malignant gliomas without p53 mutations. *Cancer Res.* **1993**, *53*, 2736–2739.
- (6) Bueso-Ramos, C. E.; Yang, Y.; deLeon, E.; McCown, P.; Stass, S. A.; Albitar, M. The human MDM-2 oncogene is overexpressed in leukemias. *Blood* **1993**, *82*, 2617–2623.
- (7) Toledo, F.; Wahl, G. M. Regulating the p53 pathway: in vitro hypotheses, in vivo veritas. *Nat. Rev. Cancer* **2006**, *6*, 909–923.
- (8) Halatsch, M. E.; Schmidt, U.; Unterberg, A.; Vougioukas, V. I. Uniform MDM2 overexpression in a panel of glioblastoma multiforme cell lines with divergent EGFR and p53 expression status. *Anticancer Res.* **2006**, *26*, 4191–4194.
- (9) Laurie, N. A.; Shih, C. S.; Dyer, M. A. Targeting MDM2 and MDMX in retinoblastoma. *Curr. Cancer Drug Targets* **2007**, *7*, 689–695.
- (10) Laurie, N. A.; Donovan, S. L.; Shih, C. S.; Zhang, J.; Mills, N.; Fuller, C.; Teunisse, A.; Lam, S.; Ramos, Y.; Mohan, A.; Johnson, D.; Wilson, M.; Rodriguez-Galindo, C.; Quarto, M.; Francoz, S.; Mendrysa, S. M.; Guy, R. K.; Marine, J. C.; Jochemsen, A. G.; Dyer, M. A. Inactivation of the p53 pathway in retinoblastoma. *Nature* **2006**, *444*, 61–66.
- (11) Mancini, F.; Conza, G. D.; Moretti, F. MDM4 (MDMX) and its Transcript Variants. *Curr. Genomics* **2009**, *10*, 42–50.
- (12) Prodromo, A.; Giglio, S.; Moretti, S.; Mancini, F.; Barbi, F.; Avenia, N.; Di Conza, G.; Schünemann, H. J.; Pistola, L.; Ludovini, V.; Sacchi, A.; Pontecorvi, A.; Puxeddu, E.; Moretti, F. Analysis of human MDM4 variants in papillary thyroid carcinomas reveals new potential markers of cancer properties. *J. Mol. Med.* **2008**, *86*, 585–596.
- (13) Patel, S.; Player, M. R. Small-molecule inhibitors of the p53-HDM2 interaction for the treatment of cancer. *Expert Opin. Invest. Drugs* **2008**, *17*, 1865–1882.
- (14) Shangary, S.; Wang, S. Small-molecule inhibitors of the MDM2-p53 protein-protein interaction to reactivate p53 function: a novel approach for cancer therapy. *Annu. Rev. Pharmacol. Toxicol.* **2009**, *49*, 223–241.
- (15) Kussie, P. H.; Gorina, S.; Marechal, V.; Elenbaas, B.; Moreau, J.; Levine, A. J.; Pavletich, N. P. Structure of the MDM2 oncoprotein bound to the p53 tumor suppressor transactivation domain. *Science* **1996**, *274*, 948–953.
- (16) Fry, D. C.; Emerson, S. D.; Palme, S.; Vu, B. T.; Liu, C. M.; Podlaski, F. NMR structure of a complex between MDM2 and a small molecule inhibitor. *J. Biomol. NMR* **2004**, *30*, 163–173.
- (17) Grasberger, B. L.; Lu, T.; Schubert, C.; Parks, D. J.; Carver, T. E.; Koblish, H. K.; Cummings, M. D.; LaFrance, L. V.; Milkiewicz, K. L.; Calvo, R. R.; Maguire, D.; Lattanze, J.; Franks, C. F.; Zhao, S.; Ramachandren, K.; Bylebyl, G. R.; Zhang, M.; Manthey, C. L.; Petrella, E. C.; Pantoliano, M. W.; Deckman, I. C.; Spurlino, J. C.; Maroney, A. C.; Tomczuk, B. E.; Molloy, C. J.; Bone, R. F. Discovery and cocrystal structure of benzodiazepinedione HDM2 antagonists that activate p53 in cells. *J. Med. Chem.* **2005**, *48*, 909–912.
- (18) Uhrinova, S.; Uhrin, D.; Powers, H.; Watt, K.; Zheleva, D.; Fischer, P.; McInnes, C.; Barlow, P. N. Structure of free MDM2 N-terminal domain reveals conformational adjustments that accompany p53-binding. *J. Mol. Biol.* **2005**, *350*, 587–598.
- (19) Fasan, R.; Dias, R. L.; Moehle, K.; Zerbe, O.; Obrecht, D.; Mittl, P. R.; Grütter, M. G.; Robinson, J. A. Structure-activity studies in a family of beta-hairpin protein epitope mimetic inhibitors of the p53-HDM2 protein-protein interaction. *ChemBioChem* **2006**, *7*, 515–526.
- (20) Sakurai, K.; Schubert, C.; Kahne, D. Crystallographic analysis of an 8-mer p53 peptide analogue complexed with MDM2. *J. Am. Chem. Soc.* **2006**, *128*, 11000–11001.
- (21) Allen, J. G.; Bourbeau, M. P.; Wohlhieter, G. E.; Bartberger, M. D.; Michelsen, K.; Hungate, R.; Gadwood, R. C.; Gaston, R. D.; Evans, B.; Mann, L. W.; Matison, M. E.; Schneider, S.; Huang, X.; Yu, D.; Andrews, P. S.; Reichelt, A.; Long, A. M.; Yakowec, P.; Yang, E. Y.; Lee, T. A.; Oliner, J. D. Discovery and optimization of chromenotriazopyrimidines as potent inhibitors of the mouse double minute 2-tumor protein 53 protein-protein interaction. *J. Med. Chem.* **2009**, *52*, 7044–7053.
- (22) Domling, A. Hot, hotter, hottest. *Cell Cycle* **2009**, *8*, 1112.
- (23) Li, C.; Pazgier, M.; Liu, M.; Lu, W. Y.; Lu, W. Apamin as a template for structure-based rational design of potent peptide activators of p53. *Angew. Chem., Int. Ed. Engl.* **2009**, *48*, 8712–8715.
- (24) Pazgier, M.; Liu, M.; Zou, G.; Yuan, W.; Li, C.; Li, C.; Li, J.; Monbo, J.; Zella, D.; Tarasov, S. G.; Lu, W. Structural basis for high-affinity peptide inhibition of p53 interactions with MDM2 and MDMX. *Proc. Natl. Acad. Sci. U.S.A.* **2009**, *106*, 4665–4670.
- (25) Phan, J.; Li, Z.; Kasprzak, A.; Li, B.; Sebt, S.; Guida, W.; Schönbrunn, E.; Chen, J. Structure-based design of high-affinity peptides inhibiting the interaction of p53 with MDM2 and MDMX. *J. Biol. Chem.* **2010**, *285*, 2174–2183.
- (26) Vassilev, L. T.; Vu, B. T.; Graves, B.; Carvajal, D.; Podlaski, F.; Filipovic, Z.; Kong, N.; Kammlott, U.; Lukacs, C.; Klein, C.; Fotouhi, N.; Liu, E. A. In vivo activation of the p53 pathway by small-molecule antagonists of MDM2. *Science* **2004**, *303*, 844–848.
- (27) Carotti, A.; Macchiarulo, A.; Giacche, N.; Pellicciari, R. Targeting the conformational transitions of MDM2 and MDMX: Insights into key residues affecting p53 recognition. *Proteins* **2009**, *77*, 524–535.
- (28) Espinoza-Fonseca, L. M.; Garcia-Machorro, J. Aromatic-aromatic interactions in the formation of the MDM2-p53 complex. *Biochem. Biophys. Res. Commun.* **2008**, *370*, 547–551.
- (29) Macchiarulo, A.; Giacche, N.; Carotti, A.; Baroni, M.; Cruciani, G.; Pellicciari, R. Targeting the conformational transitions of MDM2 and MDMX: insights into dissimilarities and similarities of p53 recognition. *J. Chem. Inf. Model.* **2008**, *48*, 1999–2009.
- (30) Lee, H. J.; Srinivasan, D.; Coomber, D.; Lane, D. P.; Verma, C. S. Modulation of the p53-MDM2 interaction by phosphorylation of Thr18: a computational study. *Cell Cycle* **2007**, *6*, 2604–2611.
- (31) Espinoza-Fonseca, L. M.; Trujillo-Ferrara, J. G. Conformational changes of the p53-binding cleft of MDM2 revealed by molecular dynamics simulations. *Biopolymers* **2006**, *83*, 365–373.
- (32) Zhong, H.; Carlson, H. A. Computational studies and peptidomimetic design for the human p53-MDM2 complex. *Proteins* **2005**, *58*, 222–234.
- (33) Dastidar, S. G.; Lane, D. P.; Verma, C. S. Modulation of p53 binding to MDM2: computational studies reveal important roles of Tyr100. *BMC Bioinformatics* **2009**, *10* Suppl. 15, S6.
- (34) Pan, Y.; Ma, B.; Levine, A. J.; Nussinov, R. Comparison of the human and worm p53 structures suggests a way for enhancing stability. *Biochemistry* **2006**, *45*, 3925–3933.
- (35) Chen, H. F.; Luo, R. Binding induced folding in p53-MDM2 complex. *J. Am. Chem. Soc.* **2007**, *129*, 2930–2937.
- (36) Dastidar, S. G.; Lane, D. P.; Verma, C. S. Multiple peptide conformations give rise to similar binding affinities: molecular simulations of p53-MDM2. *J. Am. Chem. Soc.* **2008**, *130*, 13514–13515.
- (37) Grasslin, A.; Amoreira, C.; Baldrige, K. K.; Robinson, J. A. Thermodynamic and computational studies on the binding of p53-derived peptides and peptidomimetic inhibitors to HDM2. *ChemBioChem* **2009**, *10*, 1360–1368.
- (38) Kalid, O.; Ben-Tal, N. Study of MDM2 binding to p53-analogues: affinity, helicity, and applicability to drug design. *J. Chem. Inf. Model.* **2009**, *49*, 865–876.
- (39) van Montfort, R. L.; Workman, P. Structure-based design of molecular cancer therapeutics. *Trends Biotechnol.* **2009**, *27*, 315–328.
- (40) Wade, M.; Wahl, G. M. Targeting Mdm2 and Mdmx in cancer therapy: better living through medicinal chemistry. *Mol. Cancer Res.* **2009**, *7*, 1–11.
- (41) Hu, C. Q.; Hu, Y. Z. Small molecule inhibitors of the p53-MDM2. *Curr. Med. Chem.* **2008**, *15*, 1720–1730.
- (42) Macchiarulo, A.; Pellicciari, R. MDM2/MDMX inhibitor peptide: WO2008106507. *Expert Opin. Ther. Pat.* **2009**, *19*, 721–726.
- (43) Garcia-Echeverria, C.; Chene, P.; Blommers, M. J.; Furet, P. Discovery of potent antagonists of the interaction between human double minute 2 and tumor suppressor p53. *J. Med. Chem.* **2000**, *43*, 3205–3208.
- (44) Hu, B.; Gilkes, D. M.; Chen, J. Efficient p53 activation and apoptosis by simultaneous disruption of binding to MDM2 and MDMX. *Cancer Res.* **2007**, *67*, 8810–8817.
- (45) Barakat, K.; Mane, J.; Friesen, D.; Tuszyński, J. Ensemble-based virtual screening reveals dual-inhibitors for the p53-MDM2/MDMX interactions. *J. Mol. Graphics Model.* **2010**, *28*, 555–568.
- (46) Vassilev, L. T. MDM2 inhibitors for cancer therapy. *Trends Mol. Med.* **2007**, *13*, 23–31.
- (47) Yu, S.; Qin, D.; Shangary, S.; Chen, J.; Wang, G.; Ding, K.; McEachern, D.; Qiu, S.; Nikolovska-Coleska, Z.; Miller, R.; Kang, S.; Yang, D.; Wang, S. Potent and Orally Active Small-Molecule Inhibitors of the MDM2-p53 Interaction. *J. Med. Chem.* **2009**, *52*, 7970–7973.
- (48) Shangary, S.; Ding, K.; Qiu, S.; Nikolovska-Coleska, Z.; Bauer, J. A.; Liu, M.; Wang, G.; Lu, Y.; McEachern, D.; Bernard, D.; Bradford, C. R.; Carey, T. E.; Wang, S. Reactivation of p53 by a specific MDM2 antagonist (MI-43) leads to p21-mediated cell cycle arrest and selective cell death in colon cancer. *Mol. Cancer Ther.* **2008**, *7*, 1533–1542.
- (49) Ding, K.; Lu, Y.; Nikolovska-Coleska, Z.; Wang, G.; Qiu, S.; Shangary, S.; Gao, W.; Qin, D.; Stuckey, J.; Krajewski, K.; Roller, P. P.; Wang, S. Structure-based design of spiro-oxindoles as potent, specific small-molecule inhibitors of the MDM2-p53 interaction. *J. Med. Chem.* **2006**, *49*, 3432–3435.
- (50) Shangary, S.; Qin, D.; McEachern, D.; Liu, M.; Miller, R. S.; Qiu, S.; Nikolovska-Coleska, Z.; Ding, K.; Wang, G.; Chen, J.; Bernard, D.; Zhang, J.; Lu, Y.; Gu, Q.; Shah, R. B.; Pienta, K. J.; Ling, X.; Kang, S.; Guo, M.; Sun, Y.; Yang, D.; Wang, S. Temporal activation of p53 by a specific MDM2 inhibitor is selectively toxic to tumors and leads to complete tumor growth inhibition. *Proc. Natl. Acad. Sci. U.S.A.* **2008**, *105*, 3933–3938.



- (51) Galatin, P. S.; Abraham, D. J. QSAR: hydrophobic analysis of inhibitors of the p53-mdm2 interaction. *Proteins* **2001**, *45*, 169–175.
- (52) Katsori, A. M.; Hadjipavlou-Litina, D. Chalcones in cancer: understanding their role in terms of QSAR. *Curr. Med. Chem.* **2009**, *16*, 1062–1081.
- (53) Cavasotto, C. N.; Orry, A. J. Ligand docking and structure-based virtual screening in drug discovery. *Curr. Top. Med. Chem.* **2007**, *7*, 1006–1014.
- (54) Sun, H. Pharmacophore-based virtual screening. *Curr. Med. Chem.* **2008**, *15*, 1018–1024.
- (55) Eckert, H.; Bajorath, J. Molecular similarity analysis in virtual screening: foundations, limitations and novel approaches. *Drug Discovery Today* **2007**, *12*, 225–233.
- (56) Gedeck, P.; Lewis, R. A. Exploiting QSAR models in lead optimization. *Curr. Opin. Drug Discovery Dev.* **2008**, *11*, 569–575.
- (57) Cross, S.; Cruciani, G. Molecular fields in drug discovery: getting old or reaching maturity. *Drug Discovery Today* **2010**, *15*, 23–32.
- (58) *LigPrep*, 2.3 ed.; Schrödinger, LLC: New York, NY.
- (59) Jorgensen, W.; Maxwell, D.; Tirado-Rives, J. Development and Testing of the OPLS All-Atom Force Field on Conformational Energetics and Properties of Organic Liquids. *J. Am. Chem. Soc.* **1996**, *118*, 11225–11236.
- (60) Jain, A. N. Surflex: fully automatic flexible molecular docking using a molecular similarity-based search engine. *J. Med. Chem.* **2003**, *46*, 499–511.
- (61) Cole, J. C.; Nissink, J. W. M.; Taylor, R. Protein-Ligand Docking and Virtual Screening with GOLD; In *Virtual Screening in Drug Discovery*; Shoichet, B., Alvarez, J., Eds.; Taylor & Francis CRC Press: Boca Raton, FL, 2005.
- (62) Goodford, P. J. A computational procedure for determining energetically favorable binding sites on biologically important macromolecules. *J. Med. Chem.* **1985**, *28*, 849–857.
- (63) Rogers, D.; Hopfinger, A. J. Application of Genetic Function Approximation to Quantitative Structure-Activity Relationships and Quantitative Structure-Property Relationships. *J. Chem. Inf. Comput. Sci.* **1994**, *34*, 854–866.
- (64) *Discovery Studio Modeling Environment*; release 2.5 ed.; Accelrys Software Inc.: San Diego, CA.
- (65) Hardcastle, I. R.; Ahmed, S. U.; Atkins, H.; Farnie, G.; Golding, B. T.; Griffin, R. J.; Guyenne, S.; Hutton, C.; Källblad, P.; Kemp, S. J.; Kitching, M. S.; Newell, D. R.; Norbedo, S.; Northen, J. S.; Reid, R. J.; Saravanan, K.; Willems, H. M.; Lunec, J. Small-molecule inhibitors of the MDM2-p53 protein-protein interaction based on an isoindolinone scaffold. *J. Med. Chem.* **2006**, *49*, 6209–6221.
- (66) Stoll, R.; Renner, C.; Hansen, S.; Palme, S.; Klein, C.; Belling, A.; Zeslawski, W.; Kamionka, M.; Rehm, T.; Mühlhahn, P.; Schumacher, R.; Hesse, F.; Kaluza, B.; Voelter, W.; Engh, R. A.; Holak, T. A. Chalcone derivatives antagonize interactions between the human oncoprotein MDM2 and p53. *Biochemistry* **2001**, *40*, 336–344.
- (67) Chen, L.; Yin, H.; Farooqi, B.; Sebt, S.; Hamilton, A. D.; Chen, J. p53 alpha-Helix mimetics antagonize p53/MDM2 interaction and activate p53. *Mol. Cancer Ther.* **2005**, *4*, 1019–1025.
- (68) Sippl, W. Development of biologically active compounds by combining 3D QSAR and structure-based design methods. *J. Comput.-Aided Mol. Des.* **2002**, *16*, 825–830.
- (69) Santos-Filho, O. A.; Hopfinger, A. J.; Cherkasov, A.; de Alencastro, R. B. The receptor-dependent QSAR paradigm: an overview of the current state of the art. *Med. Chem.* **2009**, *5*, 359–366.
- (70) Wells, J. A.; McClendon, C. L. Reaching for high-hanging fruit in drug discovery at protein-protein interfaces. *Nature* **2007**, *450*, 1001–1009.
- (71) Baroni, M.; Cruciani, G.; Sciabola, S.; Perruccio, F.; Mason, J. S. A common reference framework for analyzing/comparing proteins and ligands. Fingerprints for Ligands and Proteins (FLAP): theory and application. *J. Chem. Inf. Model.* **2007**, *47*, 279–294.
- (72) Friedman, J. H. Multivariate adaptive regression splines. *Ann. Stat.* **1991**, *19*, 1–141.
- (73) Johnson, S. R. The trouble with QSAR (or how I learned to stop worrying and embrace fallacy). *J. Chem. Inf. Model.* **2008**, *48*, 25–26.
- (74) Worrall, E. G.; Wawrzynow, B.; Worrall, L.; Walkinshaw, M.; Ball, K. L.; Hupp, T. R. Regulation of the E3 ubiquitin ligase activity of MDM2 by an N-terminal pseudo-substrate motif. *J. Chem. Biol.* **2009**, *2*, 113–129.
- (75) Worrall, E. G.; Worrall, L.; Blackburn, E.; Walkinshaw, M.; Hupp, T. R. The effects of phosphomimetic lid mutation on the thermostability of the N-terminal domain of MDM2. *J. Mol. Biol.* **2009**, *398*, 414–428.
- (76) Maggiora, G. M. On outliers and activity cliffs—why QSAR often disappoints. *J. Chem. Inf. Model.* **2006**, *46*, 1535.

CII00113P